

Long-term Trends in the Upper atmosphere using the incoherent scatter radar observations over Arecibo

D. Selvaraj¹, Michael P. Sulzer¹, Shun-Rong Zhang², Christiano G. M. Brum¹,
and Nestor Aponte¹

¹Arecibo Observatory, University of Central Florida (UCF), Arecibo, Puerto Rico

²Haystack Observatory, Massachusetts Institute of Technology, Westford, Massachusetts, USA

Key Points:

- Long-term trends of ion temperature at Arecibo show upper atmosphere is cooling.
- Trends of ion temperature show latitudinal dependency especially at ~ 350 km.
- Gravity waves may be one of the contributing factor to the observed cooling over Arecibo; these waves might be generated by lower atmospheric weather phenomena.

Corresponding author: Selvaraj Dharmalingam, selvaraj@naic.edu

Abstract

Upper atmospheric long-term trends could be examined in the ion temperatures (T_i) at the ionospheric F-region altitudes by the close coupling between neutrals and ions. We have analyzed the T_i data sets of Arecibo Observatory (AO) incoherent scatter radar (18°20'N, 66°45'W) from 1985 to 2019, to examine the long-term trends of the ion temperature as a function of height from ~140 km to ~677 km. For this, the responses of T_i to solar and geomagnetic activities have been taken into account as forcings of the T_i behavior as well the annual and semi-annual oscillations. By removing the known forcing that govern the T_i behavior by the difference between the T_i data and a climatological model, our results indicate that the upper atmosphere/ionosphere over Arecibo is cooling over the 35 years studied. Around 350 km, our findings also show that the rate of cooling over Arecibo is lower than previously reported for high latitudes, suggesting a latitudinal dependency. These cooling trends are believed to be the result of increasing green house gases, but the observed cooling trends exceed the magnitude of the cooling expected from green house gases. We have made an attempt to find the additional driver for observed cooling trends by linking these upper atmospheric trends to lower atmospheric weather phenomena. We found that gravity waves in the lower atmosphere associated with terrestrial weather phenomena might be contributing to the observed cooling trends in the upper atmosphere.

1 Introduction

The concentration of greenhouse gases in the lower atmosphere is increasing as a result of man-made activity. These anthropogenic greenhouse gases lead to the global warming in the lower atmosphere, but are expected to cool the upper atmosphere (Roble & Dickinson, 1989; Laštovička, 2021; Laštovička, 2015; Laštovička et al., 2006). However, this cooling could also be additionally caused by long-term changes in geomagnetic activity (Mikhailov, 2006; Liu et al., 2021), changes in the earth's magnetic field (Cnossen & Maute, 2020; Cnossen, 2014; Qian et al., 2021; Yue et al., 2018), gravity wave activities (Oliver et al., 2013; Yiğit & Medvede, 2009), and also other drivers which are in debate (Oliver et al., 2013, 2014, 2015; Laštovička, 2015).

Studies of long-term changes of the upper atmosphere/ionosphere have started after the modeling work of Roble and Dickinson (1989), who presented the changes in temperature and density from doubling of the CO₂ and CH₄ concentrations, finding both atmospheric cooling and density decreases. Also they found lowered E- and F- layer peak densities and reduction of atmospheric drag on satellites. Rishbeth (1990) also predicted a decrease in thermospheric density in response to an increase in the concentration of greenhouse gases. Long-term changes in the densities were studied using the near-Earth space objects of 1996-2001, in the height range of 200-700 km in order to understand influences by the cooling effect of increased greenhouse gases (Emmert et al., 2004). It was found that the densities are decreasing (Emmert et al., 2004, 2008, 2010; Emmert, 2015; Keating et al., 2000; Cai et al., 2019) in the range of -2% to -5% per decade at those heights as predicted by the theory. Density decrease is also seen ~350 km when the effect of solar variability was avoided by evaluating only the solar minimum years (Emmert et al., 2004).

Lowering of peak height of the F2-layer (hmF2) was found in ionospheric long-term trend studies, (Bremer, 1992; Santos et al., 2011; Brum et al., 2011), which could be associated to the changes of the meridional neutral wind component that became more poleward as reported by (Brum et al., 2012). It may be mentioned that stronger zonal winds are connected with larger gravity wave amplitudes in the mesosphere over mid-latitude (Jacobi, 2014). The long-term trends of ionosonde based studies used the values of hmF2, but changes in it could be caused not only by the neutral temperature and aforementioned winds, but possibly also by electric fields (Holt & Zhang, 2008). Holt and Zhang

(2008) pointed out a few more disadvantages in using the hmF2 for inferring the trends of neutral temperature, and also they stated that the ion temperature (T_i) is good representative of neutral temperature at certain heights where there exists a close coupling between neutrals and ion components (Holt & Zhang, 2008).

Holt and Zhang (2008) used T_i data from the Millstone Hill Incoherent Scatter Radar (ISR) from 1978 to 2007 for long-term studies, T_i and T_n (-5 K/year) from 375 km have negative trend much greater than anticipated from Roble and Dickinson (1989). This trend of T_i matches with that of the St. Santin ISR at the same altitude (Donaldson et al., 2010). Four solar cycle of Millstone Hill ISR data (1968-2006) was analysed for the long-term trend at noon in the altitude range of 100-550 km. A cooling trend was found above 200 km and it increases with altitude; also a warming trend was also found below 200 km (Zhang et al., 2011). Zhang et al. (2011) stated that their height variation patterns are in agreement with the models predicting the response of the ionosphere to the changes in concentration of greenhouse gas. Ogawa et al. (2014) have found comparable values but not exact values of observed T_i trends with the model predictions; they used the ISR observations of EISCAT UHF radar at Tromso during 1981-2013.

(Zhang & Holt, 2013) used Millstone Hill ISR data to understand the long-term cooling as functions of local time, season, solar activity and geomagnetic activity. Zhang and Holt (2013) found stronger cooling trends during daytime than nighttime. They also found negligible seasonal variation in the T_i trend, in agreement with the negligible seasonal variation in neutral density trends of Emmert et al. (2004) (Zhang & Holt, 2013). Strong cooling trends were found during solar minimum whereas less cooling or warming were found during solar maximum. It was speculated that a fraction of cooling trend was due to gradual shifting of Millstone Hill away from sub-auroral region (Zhang & Holt, 2013).

Zhang et al. (2016) analyzed two high-latitude ISR site data sets (Sondrestrom during 1990–2015, Chatanika/Poker Flat during 1976–2015 with a gap in 1983–2006) for a comprehensive study on long-term trends and also for a comparison with the Millstone Hill ISR data. Zhang et al. (2016) concluded that the upper atmosphere is cooling globally, especially above 200 km. Above 275 km, cooling trends have geomagnetic latitudinal dependency. The cooling trends were found to be much greater than the model predicted for the increase in the concentration of greenhouse gases.

Discrepancy between model predicated values and observed trends of cooling are not yet fully understood. Lack of understanding in long-term trends could be due to the limited amount of well-calibrated data and its availability (Ogawa et al., 2014). It may need further studies to understand the variability in derived cooling trends as mentioned by Zhang et al. (2016). In order to understand the long-term trend of ion temperature in the upper atmosphere and its geomagnetic latitude dependency, we made an attempt to find the long-terms trends of T_i over Arecibo using Arecibo Observatory ISR data sets from 1985-2019. And then we compared them with the long-term trends of Debye radius (L_d), Debye number (L_n) and Mean-Free-Path (L_{mfp}) for local midnight in order to understand the influence of cooling and density depletion on the plasma parameters. In order to understand the geomagnetic latitude dependency of T_i trends, we have compared the estimated T_i trends of AO-ISR (Arecibo Observatory incoherent scatter radar) with those of other ISRs.

2 Data Analysis

2.1 Estimation of T_i Residuals

We have analysed the ion temperature (T_i) from ion-line data sets which were obtained from the Arecibo Observatory Incoherent Scatter Radar (AO-ISR) (18°20'N, 66°45'W). The AO-ISR ion-line data sets were processed in different ways. We use the data which

were processed by the world day standard algorithm. These data sets are available from October 1985, and so throughout three solar cycles. We use the ISR data from 1985 to 2019 at all zenith angles; the AO-ISR could steer the beam up to 20° of off-zenith, and these data cover all the hours and months as shown in Figure 1, especially in the figure of hour vs month. No ISR data is available during 1996 and 2007 as shown in year vs hour of data distribution. There are data gaps which are represented by white/blank space in the figure of year vs month. It can be mentioned that hourly median values are used to generate this data distribution. Since AO-ISR observations had different time and altitude resolutions, altitude resolution is fixed to be ~ 36 km in order to bin the T_i data into 19 altitude bins from ~ 100 to ~ 750 km. Three altitude bins, the first bin and last two bins, were removed from further analysis since there were few data points. Hence, T_i trends are calculated for 16 altitude bins which center at 140, 176, 212, 247, 283, 319, 355, 391, 427, 462, 498, 534, 570, 606, 642, and 677.

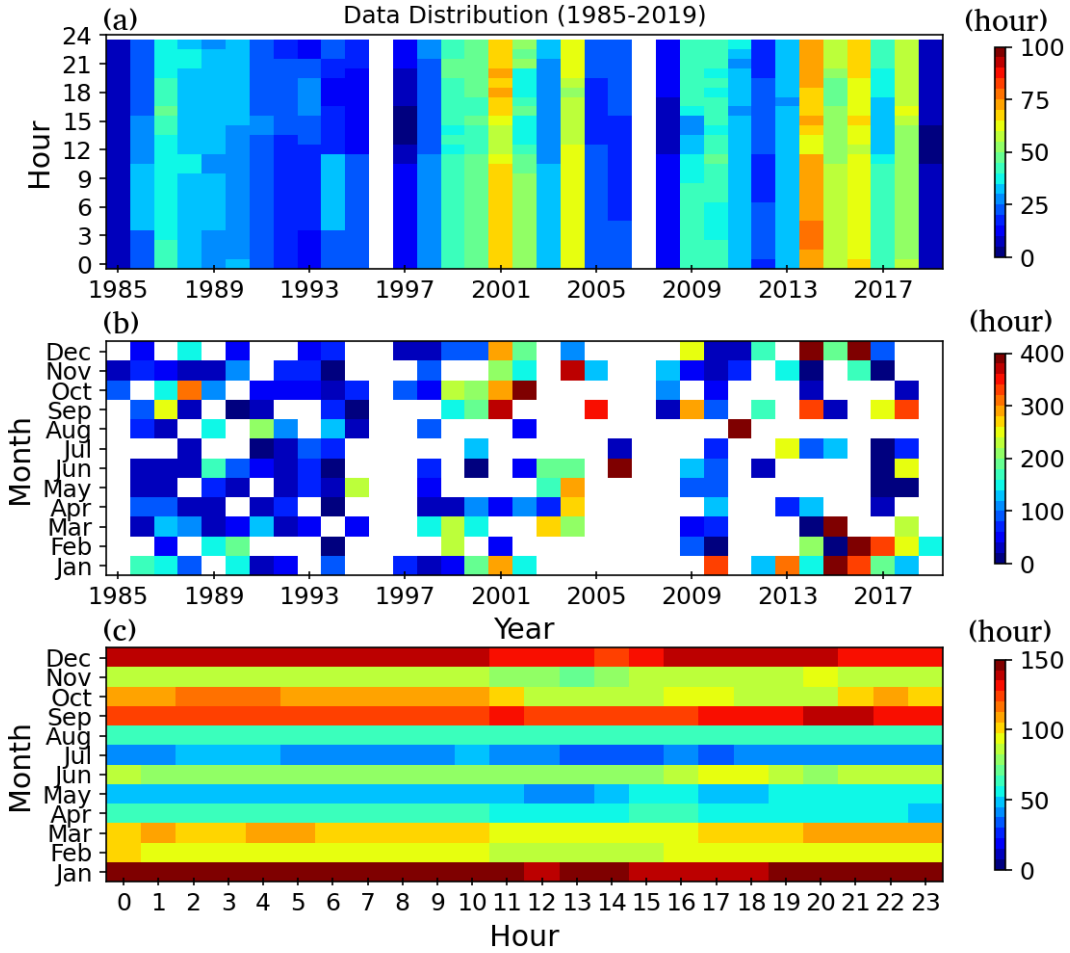


Figure 1. Temporal distribution of ion temperatures from 1985 to 2019 over Arecibo; (a) year Vs local time, (b) year Vs month, and (c) hour Vs month. The scale represents number of hours.

Climatological models could be less reliable when there are geomagnetic disturbed conditions or extremely high solar activity. In order to remove such effects, we rejected the T_i values corresponding to the solar flux at 10.7 cm at $F_{10.7} > 300$ and geomagnetic activity at $ap > 80$. Monthly median values of T_i are estimated for the T_i trend calculations in order to eliminate the issues in observations such as short-term correlations over days/hours, oversampling and outliers (Holt & Zhang, 2008; Zhang et al., 2016).

For the T_i trend calculations, minimum number of data points are set to be more than 6 points in each altitude bin. (Holt & Zhang, 2008; Zhang et al., 2016).

T_i data are binned into altitude and monthly bins for constructing a T_i model. T_i s corresponding to local mid-noon (16 UT) and mid-night (4 UT) are taken within ± 3 hours of these times for comparison between day and night, (Zhang et al., 2016).

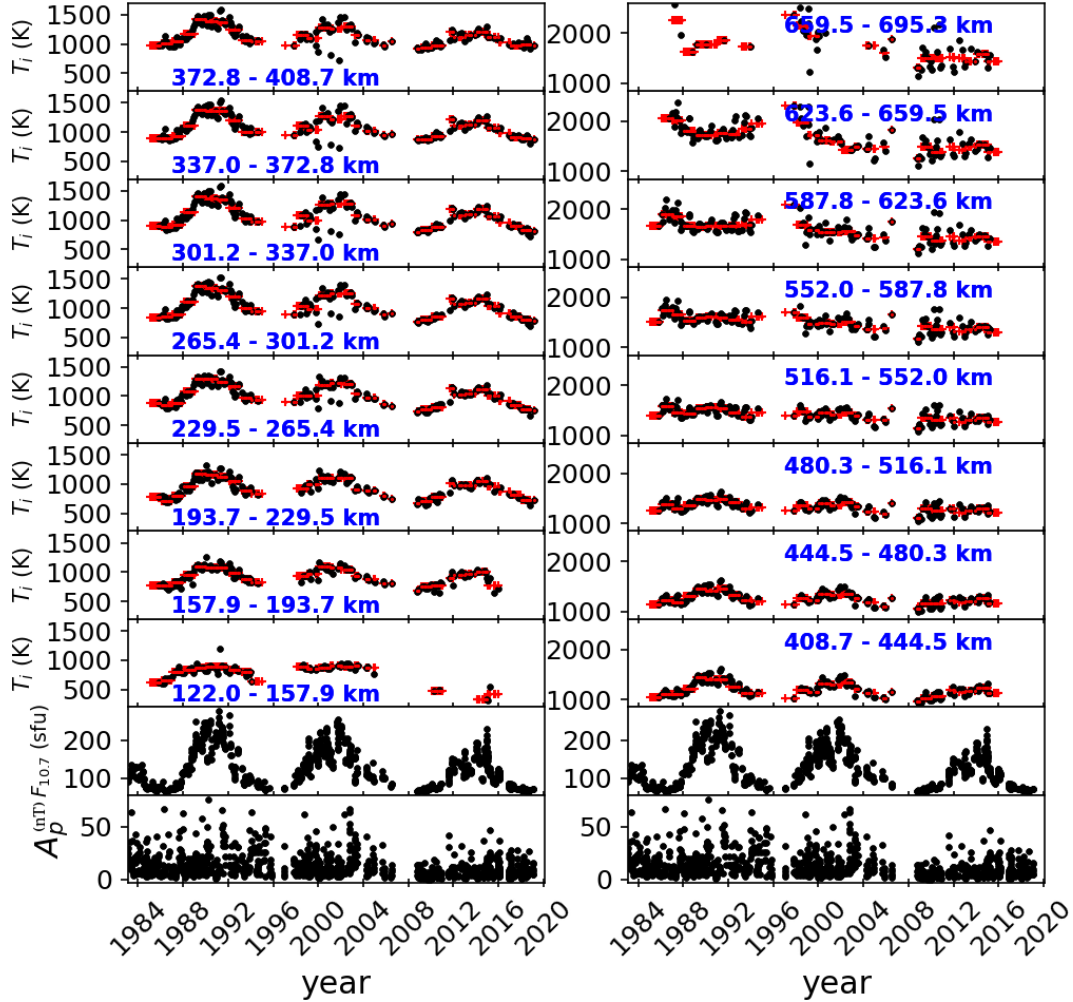


Figure 2. Monthly medians of ion temperature within ± 3 hour of local noon (black dot) at various altitudes (the red crosses represents the yearly medians). The two bottom panels of each column are solar flux and geomagnetic activity corresponding to the study period.

Figure 2 shows the monthly median of T_i (black dot) at various altitudes along with corresponding $F_{10.7}$ and A_p index. The T_i values are within ± 3 hours of local noon. Night values are not presented here but those also have similar dependence on $F_{10.7}$ and A_p index. Red-plus-symbols indicate the yearly medians. Monthly and yearly medians of ISR observed T_i have trends similar to those of the $F_{10.7}$ and A_p indices. Variation of T_i shows the strong dependence on $F_{10.7}$. This means that the influences of solar and magnetic activity on T_i need to be removed in order to reveal the trend caused by unknown drivers. It can be mentioned that continuous observations of T_i are not available for all the the day and night. So that there are data gaps, especially above ~ 620 km

in day and below ~ 200 km in night (not shown here). Those altitude ranges are included instead of removing, to have a consistency in altitude ranges during day and night.

For a given altitude bin, T_i variations are modeled for each time bin based on a least square fitting using the monthly median of the ISR observed T_i , monthly median of solar flux at 10.7 cm and monthly median of A_p index (Holt & Zhang, 2008; Zhang et al., 2011; Zhang & Holt, 2013; Zhang et al., 2016) while taking into account the annual- and semi-annual oscillations also. Variation of T_i is modeled based on the equation given by Zhang et al. (2016), as shown in Equation 1:

$$T_i = T_b + t(y - \bar{y}) + \sum_{n=1}^2 [a_n \sin(2\pi nd/365) + b_n \cos(2\pi nd/365)] + f_1(F_{10.7} - \overline{F_{10.7}}) + f_2(F_{10.7} - \overline{F_{10.7}})^2 + a(A_p - \overline{A_p}) + R \quad (1)$$

where, T_b - background constant term, y - floating-point year, \bar{y} - mean floating year, t - long-term trend, d - day number of the year, $F_{10.7}$ - monthly solar flux in sfu, $\overline{F_{10.7}}$ - mean of solar flux over entire time series, A_p - A_p index, $\overline{A_p}$ - mean of A_p index over entire time series, R - fitting residual. The coefficients T_b , t , f_1 , f_2 and a are estimated for each altitude bin by least-square fitting method.

For a given component (long-term trend / $F_{10.7}$ / A_p index), the T_i residuals are obtained by removing contribution of the other two components (estimated) from the ISR observed T_i . The detailed procedures to obtain the T_i residual are given in Holt and Zhang (2008); Zhang et al. (2011); Zhang and Holt (2013); Zhang et al. (2016). In order to make the comparison of T_i trends among the ISR sites, a similar method has been used in this study for error estimations also as in Holt and Zhang (2008); Zhang et al. (2011); Zhang and Holt (2013); Zhang et al. (2016). In error estimation, 10000 bootstrap samples are used in order to compute the errors in 95% confidence intervals.

2.2 Estimation of Debye Parameters, Mean-Free-Path and its Residuals

Debye radius (L_d), Debye number (L_n) and Mean-Free-Path (L_{mfp}) are calculated at the condition of thermal equilibrium when ratio of electron temperature to ion temperature is one. Since it occurs at nighttime; we have calculated the Debye radius (L_d), Debye number (L_n) and Mean-Free-Path (L_{mfp}) for local mid-night (4 UT) with ± 3 hour by following the Equations 2, 3, and 4 given by Livadiotis (2019); Goldston and Rutherford (1995)

$$L_d = \sqrt{\frac{\epsilon_0 k_B T_e}{N_e e^2}} \quad (2)$$

$$L_n = \frac{4\pi}{3} N_e L_d^3 \quad (3)$$

$$L_{mfp} = \frac{64\sqrt{6}\pi\epsilon_0^2(k_B T_e)^2}{e^4 N_e \ln(9L_n)} \quad (4)$$

where ϵ_0 is the free space permittivity, k_B is the Boltzmann constant, T_e is the electron temperature, N_e is the ISR retrieved electron density, and e is the charge of electron.

In order to calculate the trend residual of L_d , L_n , and L_{mfp} , we have used the Equation 1 by replacing the temperature term with L_d , L_n , and L_{mfp} , respectively. Also a negative sign was assigned in the equation for solar the flux and A_p index, since a negative correlation coefficient is found in relation with L_d , L_n , and L_{mfp} , even though it is small value as shown in Figure 3.

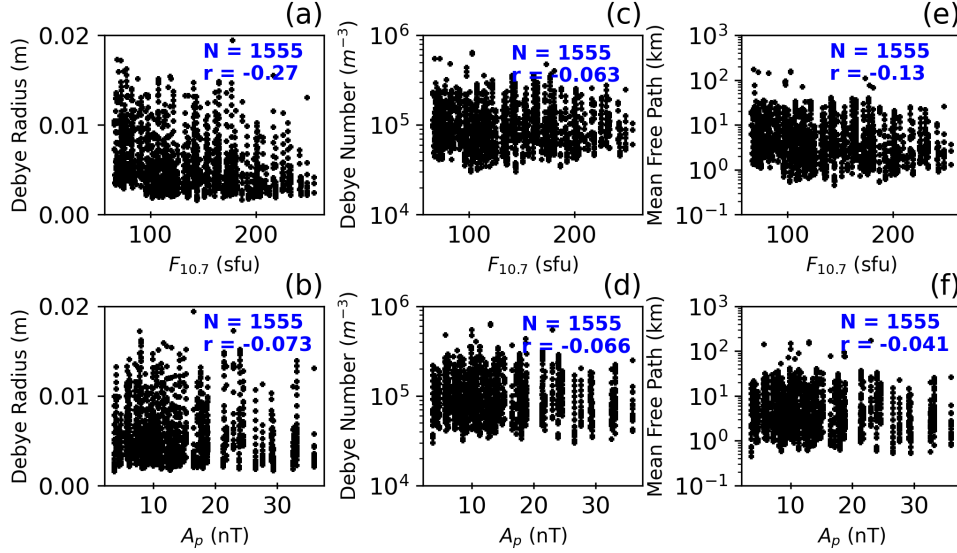


Figure 3. Dispersion diagram of L_d , L_n , and L_{mfp} against solar flux ($F_{10.7}$) and geomagnetic activity (A_p index) (upper and bottom rows, respectively). (a) $F_{10.7}$ Vs L_d , (b) A_p Vs L_d , (c) $F_{10.7}$ Vs L_n , (d) A_p Vs L_n , (e) $F_{10.7}$ Vs L_{mfp} , (f) A_p Vs L_{mfp} ,

3 Results

3.1 T_i trend and dependency of T_i on solar activity and geomagnetic activity

The T_i residuals are presented in Figure 4 for daytime. The T_i residuals are calculated by removing the contributions from annual, semi-annual oscillation, as well as solar and geomagnetic activity. In Figure 4, T_i residuals (monthly median-black and yearly median-green) are shown at various altitudes from ~ 122 -700 km along with number of months (No.), trend line (solid black line) and its slope (m), error (confidence level of 95%), and correlation coefficient (r) between T_i and floating year. T_i residuals spread around the trend line which means that those residuals are origin of ionospheric weather rather than statistical noise. Altitudes above ~ 480 km are having larger errors (~ 2 K/year) relatively than lower altitudes. Other than the highest altitude which does not have enough data points to represent the 3 solar cycles, the largest error is found to be -5.98 corresponding to 67 points at the altitude bin of ~ 623.6 -659.5 km. Most of the times, very large errors are associated with too few data points. In order to eliminate such bias in interpretation, we have removed the trends of those altitudes (day: ~ 516.1 -695.3 km; night: ~ 122 -193.7 km) in further analysis whose errors are more (< -2.7 which is the allowed largest error taken from largest error nighttime). Even with the the large error, we preserve the altitude of 122-157.9 km during daytime which has positive trend (for sake of discussion).

All the altitudes having the cooling T_i trends, which vary from -0.31 K/year to -9.96 K/year during the daytime except the altitude bin of ~ 122 -158 km. Strong cooling of -9.96 K/year occurs at the altitude bin of ~ 623.6 -659.5 km where high errors are seen. Weakest cooling of -0.31 K/year occurring at ~ 193.7 -229.5 km with error of 0.56 K/year.

T_i residuals during nighttime for components of year is shown in figure 5. First two lower altitude bins (~ 122 -158 km & ~ 158 -194 km) fewer than 60 samples. In the altitude bin of ~ 194 -230 km, a weak warming trend is found. Above ~ 230 km, cooling

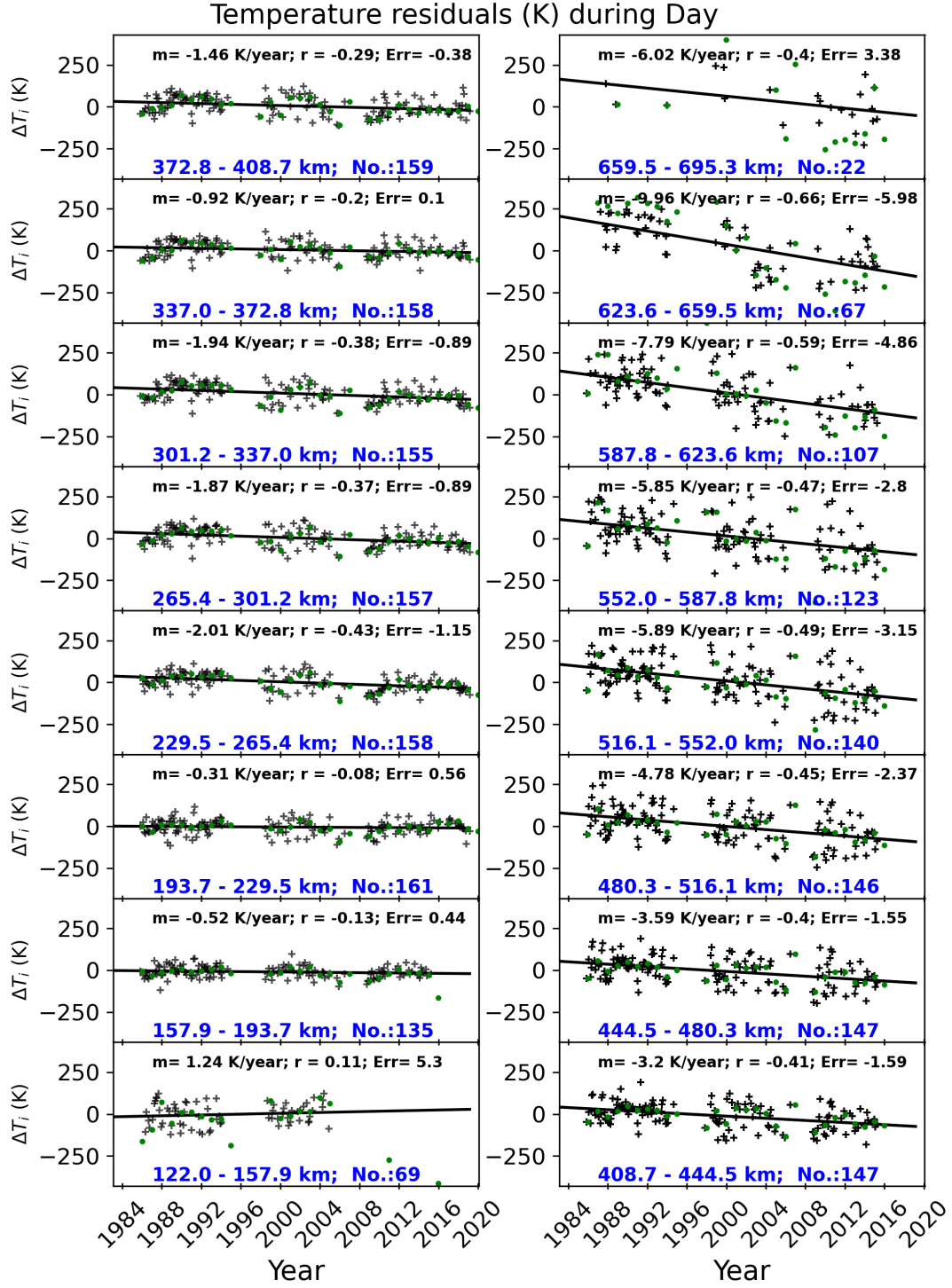


Figure 4. Daytime T_i Residuals as a function of year and altitude along with trend line (black solid line) and its statistics (slope (m), standard error (Err), and correlation coefficient (r) between T_i and floating year). Monthly medians are in black crosses and yearly medians are in green crosses.

trends are gradually increasing as a function of altitude. These cooling T_i trends vary from -0.54 K/year to -4.59 K/year during the nighttime. Strong cooling of -4.59 K/year occurring at the altitude bin of ~ 623.6 -659.5 km where the strong cooling is also found during daytime, but with a different magnitude. Weakest cooling of -0.54 K/year occurs at the altitude bin of ~ 337 -372.8 km with error of 0.32 K/year. The T_i residuals for the components of $F_{10.7}$ and A_p have been calculated for each altitude as in figure 4 & 5 but are not shown here. Indeed, the ratios $\delta T_i / \delta f_{10.7}$ (K/sfu) and $\delta T_i / \delta A_p$ (K/ap) are shown as function of altitude along with T_i trends in Figure 6.

In Figure 6, the estimated T_i trends, the $F_{10.7}$ and to the A_p index for day (red) and night (black) are presented as function of altitude, (a) T_i trend (K/year), (b) $\delta T_i / \delta f_{10.7}$ (K/sfu), and (c) $\delta T_i / \delta A_p$ (K/ap). Large errors are found to occur in the lower altitudes (less than ~ 200 km) during nighttime whereas the same do occur in the higher altitudes during daytime. T_i trends are negative in all the altitude ranges except the lower altitude bin of ~ 122 -158 km during daytime and ~ 194 -230 km during nighttime. Estimated T_i trends are varying from -0.63 K/year to -13.5 K/year, indicating the cooling trend overall ionosphere during day and night. T_i trends are almost comparable between day and night in the altitude range of ~ 200 -450 km even though the cooling trends are little stronger in daytime than nighttime. Above 480 km, T_i trends of nighttime show the less cooling than daytime.

Figure 6(b) shows the altitude variation of $\delta T_i / \delta f_{10.7}$ (K/sfu). In order to check the linear relation between δT_i and $\delta f_{10.7}$, we have calculated the linear correlation coefficient between them. A strong linear relationship is found between T_i residuals and $F_{10.7}$. The large values of positive linear correlation coefficients (r) are varying from 0.77 to 0.93 within the altitude range of ~ 158 -445 km during daytime. The linear relationship is positive from ~ 120 km to ~ 550 km during daytime whereas the this positive relationship is found to occur in all the altitudes during nighttime. During daytime, $\delta T_i / \delta f_{10.7}$ (K/sfu) are large around 310 km where electron density peaks during daytime, and gradual decrease is found to occur around that altitude, similar to electron density profile. It might be due to electron heating of the the ions through collisions. This altitude variation of $\delta T_i / \delta f_{10.7}$ (K/sfu) during daytime is consistent with results of Sondrestrom Zhang et al. (2016). During nighttime, the large values of positive linear correlation coefficients(r) are varying from 0.76 to 0.95 within the altitude range of ~ 230 -695 km. And also $\delta T_i / \delta f_{10.7}$ (K/sfu) are increasing gradually as a function of altitude. Profiles of $\delta T_i / \delta f_{10.7}$ (K/sfu) are not the same during day and night. Above the peak altitude of ~ 300 km, the daytime profile of $\delta T_i / \delta f_{10.7}$ (K/sfu) is decreasing as a function of altitude whereas it is increasing as a function of altitude during nighttime. It probably means that the solar activity influences the ion temperatures uniformly in the altitude range of ~ 200 -700 km during nighttime. Whereas, solar activity influences are different on ion temperatures in each altitude during daytime. These day and night variability of $\delta T_i / \delta f_{10.7}$ are different from Sondrestrom since Sondrestrom observed the same feature of variability between day and night but with different magnitude (Zhang et al., 2016). In comparison, T_i is sensitive to $F_{10.7}$ in the altitude range of ~ 200 -400 km during day whereas nighttime T_i is sensitive to $F_{10.7}$ above ~ 400 km.

Figure 6(c) shows the altitude variation of $\delta T_i / \delta A_p$ (K/ap). In order to check the linear relation between δT_i and δA_p , we have calculated the linear correlation coefficient (r) between them. The linear relationship is found to be not strong between T_i residuals and A_p since the positive-maximum of r is 0.11 (day) and 0.42 (night). Large values of r are occurring around ~ 300 km where peak electron density may appear; it might be due to T_i is sensitive to A_p . By neglecting the large error altitudes, $\delta T_i / \delta A_p$ (K/ap) is decreasing as a function of altitude above ~ 300 km during daytime and it is increasing as a function of altitude above ~ 337 km during nighttime. These day and night variability of $\delta T_i / \delta A_p$ are different from Sondrestrom and Poker Flat since Sondrestrom and Poker Flat observed the same feature of variability between day and night but with

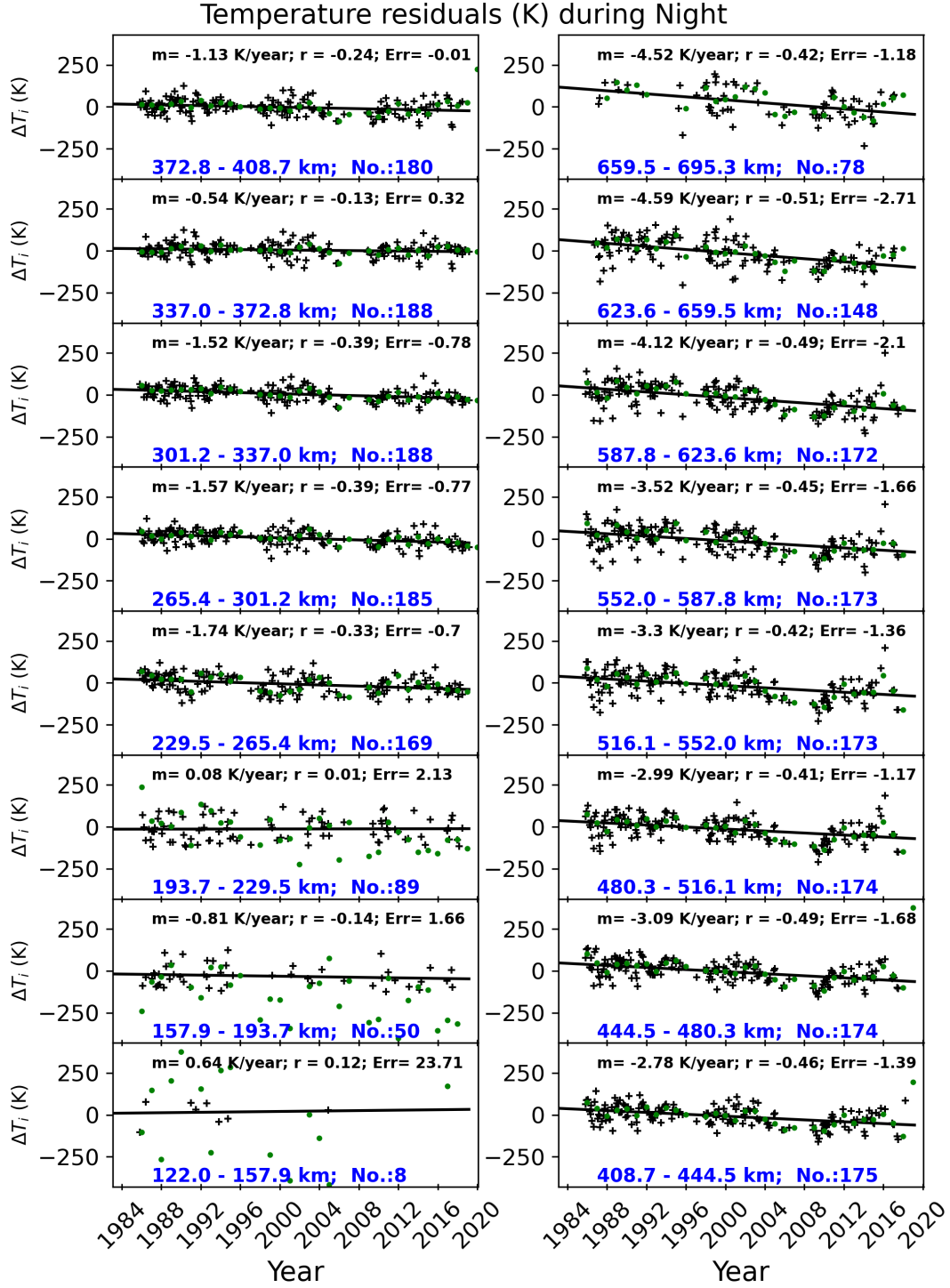


Figure 5. Similar to Figure 4 but for nighttime period.

different magnitude (Zhang et al., 2016). In comparison, T_i is sensitive to A_p during night-time than daytime. Probably, it might be due to the absence of polar cusp influences.

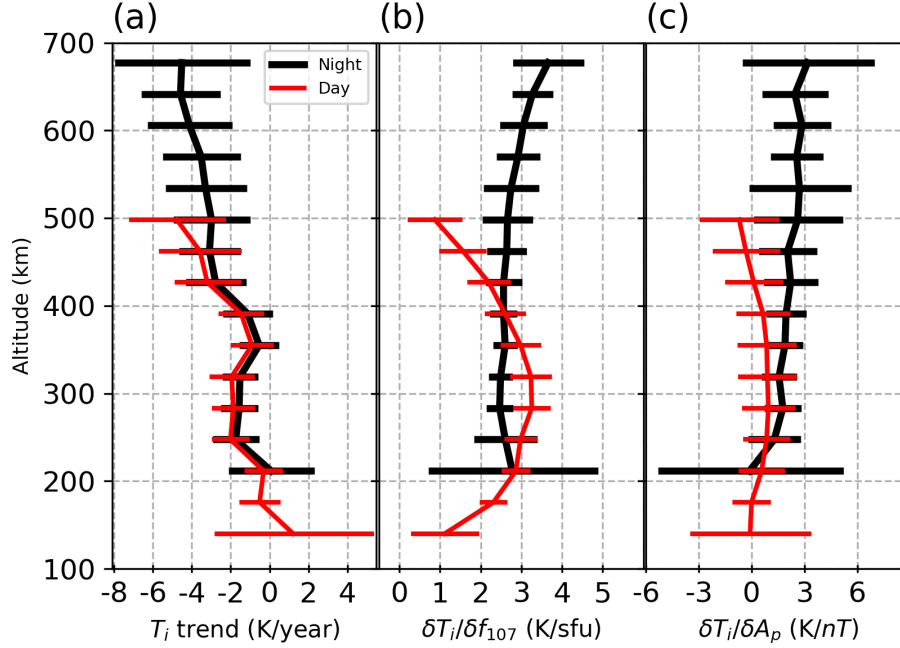


Figure 6. T_i trend (a) and T_i response to $F_{10.7}$ expressed as $\delta T_i / \delta f_{10.7}$ (K/sfu) (b) and A_p expressed as $\delta T_i / \delta A_p$ (K/nT) (c) for day (red) and night (black) as function of altitude.

3.2 Mean Free Path

To understand the effect of cooling trends on other plasma parameters of ionosphere/upper atmosphere, we have estimated the Debye radius (L_d), Debye number (L_n), and Mean-Free-Path (L_{mfp}) at thermal equilibrium using the Equations 2, 3, and 4, respectively. Estimations are made for nighttime since thermal equilibrium occurs during this period. Figure 7 shows the altitudinal variations of median plasma parameters with 25th & 75th percentiles (a) T_i/T_e (K) & N_e (m^{-3}), (b) L_d (m), and (c) L_n (m^{-3}) & L_{mfp} (km). Statistical estimation of median, 25th & 75th percentiles are calculated using all the samples of 1985-2019. In Figure 7(a), red-and-black and blue color lines represent the electron-and-ion temperature and electron density, respectively. F-region's electron densities are start to increase from ~ 175 km ($\sim 1.3 \times 10^{10} m^{-3}$); it attains maximum density of $\sim 4 \times 10^{11} m^{-3}$ at ~ 350 km; and it decreases gradually as function of altitude above ~ 350 . F-region's electron/ion temperatures start to increase from ~ 175 km (~ 625 K); it increases rapidly to ~ 875 K at ~ 250 km; and then it increases gradually above the altitude of ~ 250 . It can be mentioned T_e and N_e are taken for analysis at nighttime when there is thermal equilibrium so that T_i are very close to T_e over Arecibo. In Figure 7(b) and (c), Debye radius/number (red) and mean-free-path (blue) are shown in red and blue, respectively. As like F-region's electron density profile, Debye radius and mean-free-path are starting to decrease from ~ 175 km to ~ 350 km (~ 0.015 m to ~ 0.0025 m & ~ 17 km to ~ 1.9 km); and then both are increasing gradually above the altitude of ~ 350 km. In figure 7(c), altitude variation of Debye number is very similar to mean-free-path and Debye radius. It is also decreasing from ~ 175 km to ~ 350 km ($\sim 1.5 \times 10^5 m^{-3}$ to $\sim 7.5 \times 10^4 m^{-3}$); and then it increases gradually above ~ 350 km.

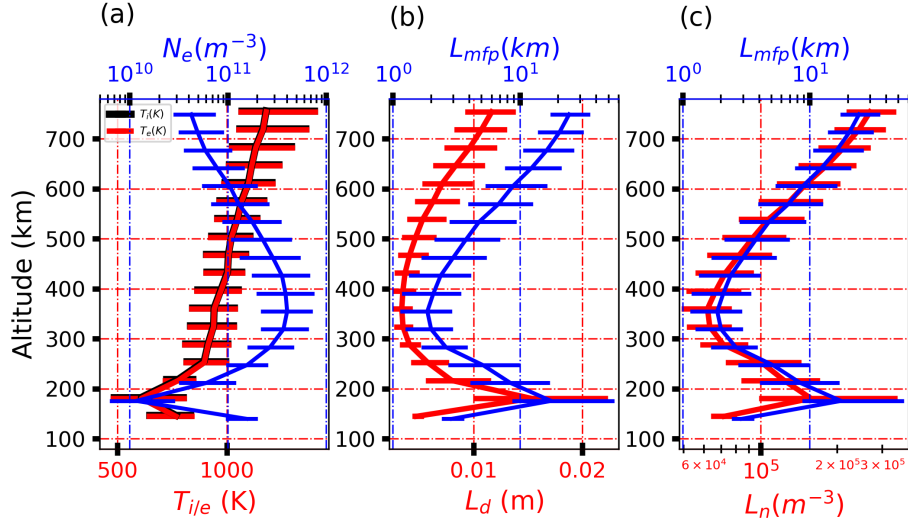


Figure 7. Altitude variations of plasma parameters for nighttime. (a) T_i/T_e (K) & N_e (m^{-3}), (b) L_d (m) & L_{mfp} (km), and (c) L_n (m^{-3}) & L_{mfp} (km).

Figure 8 shows the residual of Debye radius for the component of year (left-side panels), $F_{10.7}$ (middle panels) and A_p (right-side panels). Debye radius trend (left-side panels) varies in the range of -0.0027 mm/year to 0.0193 mm/year. High positive trend is coinciding the altitude of maximum electron density in F-region at altitude bin of ~ 337 -373 km. Large magnitudes in confidence level of 95 % indicate more errors. Debye radius residuals for the component of $F_{10.7}$ (middle panels) varies in the range of -0.0108 mm/sfu to -0.0297 mm/year. Linear correlation coefficient (r) between Debye radius residuals and $F_{10.7}$, varies from -0.49 to 0.72; it might be due to Debye radius is sensitive and negatively respond to $F_{10.7}$. Whereas the linear correlation coefficient (r) of Debye radius residuals with year and A_p varies close to zero. Debye radius might be not sensitive to A_p . The nature of linear correlation for Debye radius, Debye number and mean-free-path residuals with $F_{10.7}$ and A_p are same as shown in Figure 8.

Sensitivity of solar activity and geomagnetic activity on ion temperature, Debye radius, Debye number and mean-free-path are examined. These influences on those parameters are removed to estimate the long-term trend. The long-term trends are found to be non-zero in those parameters, which indicates a role of an unresolved driver. Investigation to search for this driver is a separate study. Here, we concentrate on the relation among ion temperature, Debye radius, Debye number and mean-free-path to understand the influence of long-term changes on background plasma parameters. In order to compare them, the altitude profiles of trends are shown in Figure 9. In this figure the trend of (a) Debye radius (red), (b) Debye number (red) and (c) mean-free-path (red) are shown along with T_i trends (blue) during night. Debye radius is increasing in the altitude ranges of ~ 240 -500 km, varying as much as 0.017 mm/year. The maximum values occur at ~ 350 and ~ 500 km. Above ~ 500 km, Debye radius shrinks as a function of altitude. In the F-region, weaker cooling trends occur at the altitude (~ 350) of peak electron density where the Debye radius is increasing. But simple a relation could not be found between the Debye radius trend and the T_i trend since there is an enlargement in Debye radius at the altitudes of ~ 400 -500 km where cooling trends are increasing as a function of altitude. In Figure 9(b), Debye number trends are negative in all the altitudes except the altitude of peak electron density (~ 350). At ~ 350 , Debye number trend found to be 40 No./year. Above and below the peak altitude of ~ 350 , the number of particles in Debye sphere is decreasing with time. Negative trend of Debye num-

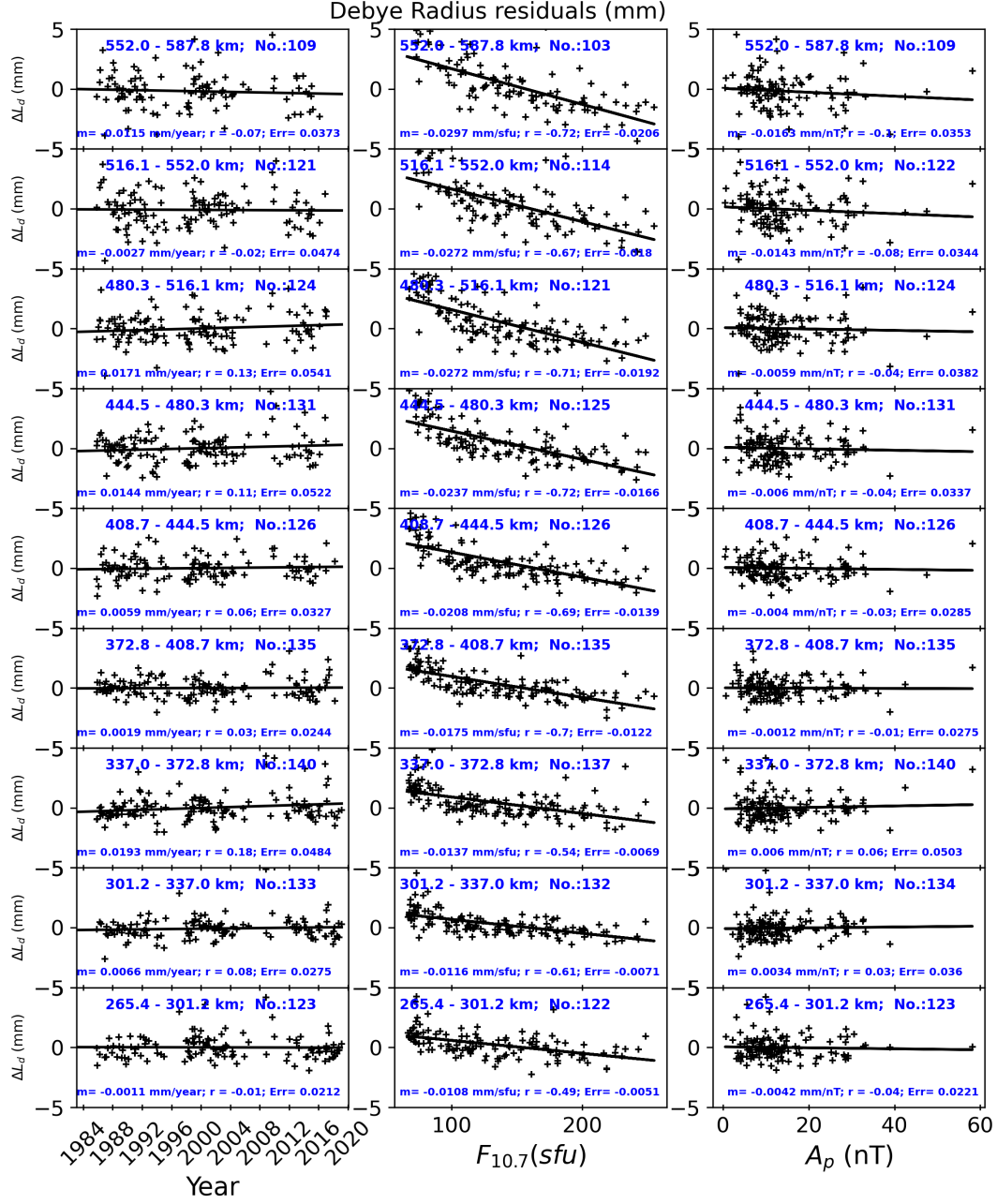


Figure 8. Debye Radius residuals for the component of year, $F_{10.7}$ and A_p .

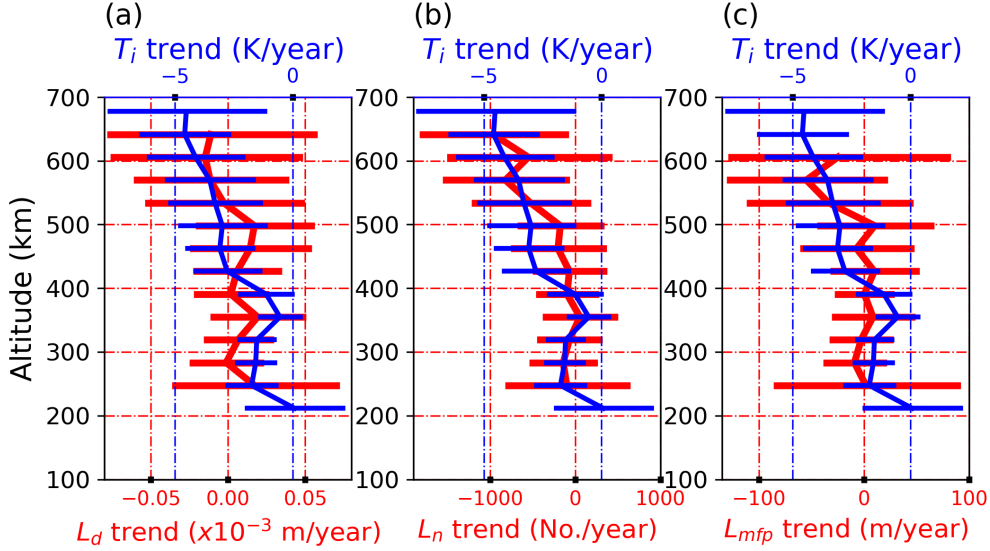


Figure 9. The trend of Debye radius, Debye number and mean-free-path.

ber is decreasing from -135 per year (at ~ 280) to 40 per year (at ~ 350) as a function of altitude at the bottom of F-region where the profile of electron density has a positive gradient. Whereas, the negative trend of Debye number is increasing as a function of altitude in the upper portion of F-region (above ~ 350) to -920 per year (~ 640) where profile of electron density has negative gradient. Overall trends of Debye number follow the altitude profile of electron density structure. The trend of Debye number and ion temperature have the similar altitude variations and both show the increasing negative-trends above the peak electron density altitude. Figure 9(c) shows the profile of mean-free-path trend. The trend of mean-free-path varying around zero from -9 m/year to 9 m/year in the altitude range of ~ 280 -500. Above ~ 500 , the mean-free-path trends are negative; this suggests that the mean-free-path is decreasing over year at those altitudes. The negative trend of mean-free-path is decreasing from -9 m/year (at ~ 280) to 8 m/year (at ~ 350) as a function of altitude at the bottom of F-region where profile of electron density has positive gradient. The trends of mean-free-path at positive gradient of F-region have a similar nature to the trend of Debye radius and number. Long-term trends suggest that there are not only the changes in T_i over time, but also changes in other plasma parameters such as Debye radius, Debye number and mean-free-path.

Long-term trends of the ion temperature from multiple ISR locations show variations in magnetic latitude. It is useful to compare the AO-ISR trends with those reported from other ISRs because it is at geomagnetic midlatitudes, while the others are higher in latitude. Figure 10 shows the comparison of long term trends of T_i among various ISR locations (pink-daytime AO, gray-nighttime AO, red-Millstone, green-St. Santin, black-Poker Flat, and blue-Sondrestorm). In Figure 10(a) ISRs observed T_i trend variations (daytime) are shown as function of altitude along with nighttime AO-ISR. Other ISR trend data are from Zhang et al. (2016). The cooling trends are observed above 200 km. Almost all cooling trends are increasing as increasing altitude. The warming T_i trends are observed within the altitude range of 150-200 km in other ISR locations than Arecibo. Over Arecibo, the cooling trend is seen in that particular altitude range but is small and the trend appears to be positive below. It may need further studies in order to understand it better. Zhang et al. (2016) observed cooling trend increases with increasing magnetic latitudes above 275 km. It is clearly seen around 350 km (as shown in Figure 10b). Above 475 km, AO-ISR observed the rapid cooling trends as a function of altitude dur-

ing daytime than night time. Unfortunately, other ISRs are limited to 475 km and the AO-ISR trend estimation shows enhanced uncertainty at high altitudes. Over Arecibo, the nighttime trends are warmer relatively than daytime. This rapid cooling above 475 km needs further study to understand the mechanism behind of it.

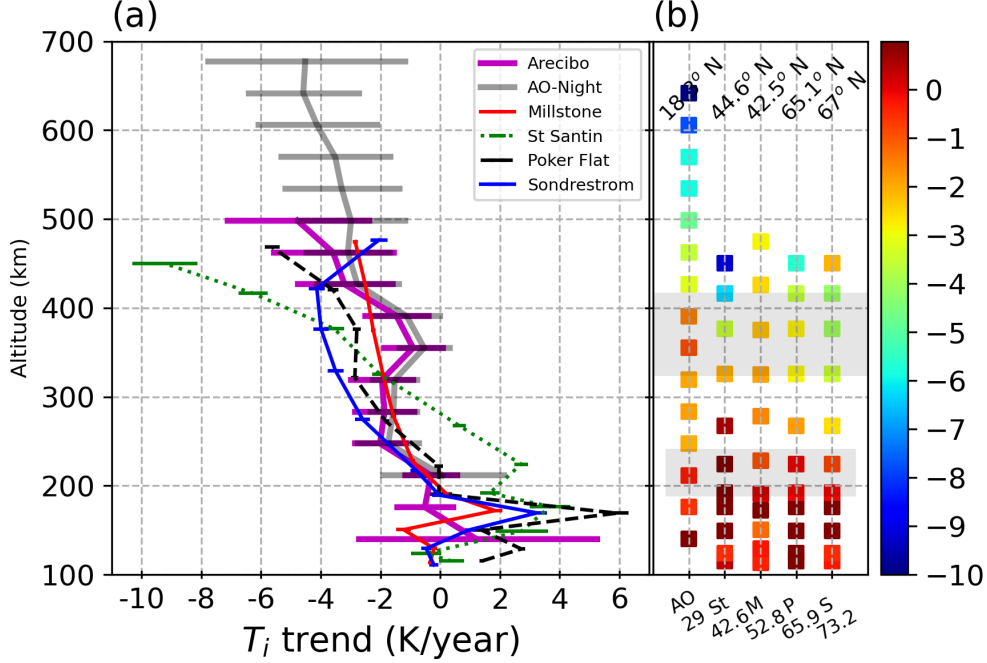


Figure 10. Comparison of T_i trend variations among the ISRs, namely, Millstone (red), St. Santin (green), Poker Flat (black), Sondrestorm (blue) and Arecibo (pink-day & gray-night). (a) T_i trend (K/year) as a function of altitude, (b) T_i trend (K/year) as a function of altitude and latitude.

3.3 Summary and Discussion

We have studied the long term trends in ion temperature using incoherent scatter data from the Arecibo observatory from 1985 to 2019. We have compared the trends to those from other ISR sites and discussed possible drivers causing the cooling trends. The following is a list of our results:

1. Ion temperatures (T_i) are found to be sensitive to solar activity (represented by the $F_{10.7}$ flux) during both day and night. The daytime T_i solar dependence has a maximum at the altitudes of the F2 peak (~ 310 km). During nighttime, T_i solar dependence increases with altitude from about 2.2 K/sfu at ~ 300 km to 3.5 K/sfu at ~ 675 km.
2. The same method used to retrieve the T_i 's dependence on solar activity was applied for its geomagnetic activity responses, but now in respect to A_p index. Little positive or non-responses of daytime T_i variation on geomagnetic activity was detected at Arecibo. On the other hand, as seen in Figure 6 (panel c), nocturnal T_i increases with the increase of A_p . Similarly, the solar activity, the T_i response to A_p increases with altitude from no responses at ~ 200 km to ~ 3 K/nT at altitudes of ~ 675 km.
3. To obtain the T_i trends, the residuals are computed by removing the variations in T_i caused by solar and geomagnetic activity, the annual- and semi-annual sea-

- sonal components. For daytime, it was found warming trend at low altitude (this altitude has more error but retained for sake of discussion) and this trend becomes more negative (cooling) with the increase of altitude. Similar behavior is seen for the nighttime period where cooling trend is increasing with altitude, reaching a maximum of -4K/year. Generally, the cooling trends are increasing as a function of altitude.
4. Cooling trends in the F-region might be caused by one or more drivers other than $F_{10.7}$, A_p , annual- and semi-annual oscillations. Further investigations are needed to find the responsible driver(s) for such trends.
 5. Cooling trend is almost the same for day and night up to the altitude of ~ 475 km with a maximum of -3.6 K/year but cooling is relatively stronger in daytime than nighttime. Above ~ 475 km, cooling trend is much stronger during daytime than nighttime.
 6. To gain further understanding on the influence of long-term trends in background parameters of ionosphere/upper atmosphere, we have performed a similar analysis on Debye radius (L_d), Debye number (L_n) and mean-free-path (L_{mfp}).
 7. We calculated the linear correlation coefficients for L_d with $F_{10.7}$ & A_p , L_n with $F_{10.7}$ & A_p , and L_{mfp} with $F_{10.7}$ & A_p . These correlation coefficients suggest that Debye radius, Debye number and mean-free-path are sensitive to $F_{10.7}$ than A_p .
 8. The trends of Debye radius, Debye number and mean-free-path might be derived in the F-region by a driver(s) other than $F_{10.7}$, A_p , annual- and semi-annual oscillations since there were a non-zero trends after removing their contributions.
 9. The Debye radius is increasing over year up to the altitude of ~ 550 km with a maximum rate of 0.017 mm/year. This maximum occurs at two altitude ranges; one is around the peak altitude of nighttime F-region (~ 350 km) and the other is at ~ 500 km. Above ~ 550 km, Debye radius shrinks and the rate of shrinking increases as a function of altitude. Further, altitude variations of Debye radius trend show possible direct relation with T_i trend around and below the peak altitude.
 10. The Debye number decreases over time and this decreasing rate is increasing as a function of altitude above peak altitude of nighttime F-region. This decreasing rate is stronger above the peak altitude than below it. Altitude variations of the number trend show the direct relation with T_i trend around and below the peak altitude, and also relative variation above that altitude.
 11. The Mean-Free-Path trends vary around zero but having the non-zero values. Altitude variations the Mean-Free-Path trend show the direct relation with T_i trend around and below the peak altitude. Above the peak altitude, the relationship is not direct/simple.
 12. Comparison of T_i trends among ISRs reveals that there are both unique features in location/latitude and commonalities. In Mid- and high-latitudes, warming trends are confined below ~ 180 km to the E-region except St. Santin, which shows the warming trend up to the altitude of ~ 275 km.
 13. Above 200 km, cooling trends are increasing as a function of altitude.
 14. Relatively, the similar values of T_i trends and also the similar vertical gradient in T_i trends are found to be in the altitudes range of ~ 180 -250 km except St. Santin.
 15. T_i trends have latitudinal dependency above 250 km.

Monthly medians of ion temperature residuals have a linear trend along with the superimposition of variations with time scales varying from 6 years to 11 years. These variations are possibly related to the decadal activity of El Niño-Southern Oscillation (ENSO) (Oliver et al., 2013). Connection between ENSO MEI index and T_i trends is discussed later. Also there are variations with time scales of ~ 16 years reported by Ogawa et al. (2014). Most of the linear T_i trends are cooling trends. Cooling trends from ion temperature residuals are found to be in all the altitudes of ionosphere/upper atmosphere except its low altitudes. At lower altitudes of ionospheric F-region, the warming trends

are observed as like mid- and high- latitudes but in different altitudes. During daytime, warming trends are below 200 km in Millstone Hill, Sondrestorm, Chatanika/Poker Flat and Saint Santin (Zhang et al., 2011, 2016; Donaldson et al., 2010). Occurrence of warming trend altitude at AO (mid-latitude station) going down to below 150 km (~ 122 -158 km) during daytime, lower in height than any other locations. It can be noted that this altitude is the lowest altitude in this study and having just enough data points of 69 months. Warming trends were also observed during nighttime at lower altitudes of ionospheric F-region as like daytime. During nighttime, Millstone Hill has the warming trends below 350 km (Zhang & Holt, 2013); Sondrestorm has it below 250 km but Chatanika/Poker Flat do not have data below 220 km and no warming was observed above 220 km (Zhang et al., 2016). These warming trends at fixed altitudes are not due to the true warming of ionosphere; it is due to downward shift in pressure level because of subsidence of the warmer air with a substantial altitude gradient in temperature as is the case for lower F-region (Akmaev & Fomichev, 1998; Donaldson et al., 2010; Zhang et al., 2011; Zhang & Holt, 2013; Zhang et al., 2016). These warming trends are occurring at lowest altitudes during daytime whereas it occurs at higher altitudes during nighttime. These occurrences are same in all the latitudes stations except Tromso (Ogawa et al., 2014; Zhang et al., 2016).

Generally above the altitudes of 200 km, cooling trends are observed in all the latitudes (Donaldson et al., 2010; Zhang et al., 2011; Zhang & Holt, 2013; Zhang et al., 2016) except high-latitude-station Tromso where warming was observed above 400 km (Ogawa et al., 2014). It can also be mentioned that cooling trends are increasing with altitude over Tromso from 230 km to 330 km. Above 330 km, cooling trends are decreasing as a function of altitude and the trends turn into warming at just 410 km. The warming trends increase above 410 km as a function of altitude (Ogawa et al., 2014). Decrease of cooling trend as a function of altitude was observed in other latitudes too but in different altitude ranges. It was observed as 325(night)/425(day)-450 km over Sondrestrom, 325-375 km over Chatanika/Poker Flat, and 266-373 km over Arecibo. These kind of reduced cooling trends in altitude profiles more or less occurring at peak altitude of F-region. It can be noted that Millstone Hill does not observe any such feature. Rather, Millstone Hill observed increasing of cooling trends as a function of altitude which is found to be in overall trends of Saint Santin, Chatanika/Poker Flat and Arecibo too. Whereas, warming trends were observed above the peak altitude of F-region over Tromso (above 400 km) during daytime (Ogawa et al., 2014).

Comparison of T_i trends during day and night reveals that the trends are closely similar values up to the altitude of 430 km over Arecibo. Whereas, the large difference were observed over Millstone Hill, Sondrestrom, and Chatanika/Poker Flat (Zhang & Holt, 2013; Zhang et al., 2016). Strong coolings are occurring during day than night in overall altitudes over Sondrestrom and Arecibo. It was other way around over Chatanika/Poker Flat such as strong cooling during night than day. Over Millstone Hill, Strong coolings were observed during day than night up to the altitude of 450 km. Above the altitude of 450 km, it gets into flip as strong cooling during night than day. It can be noted that comparable cooling is observed ~ 475 km over Millstone Hill which are observed over Arecibo below this said altitude. It needs further study to find the explanations why the difference should occur between both stations at mid-latitudes. Above the altitude of 475 km, daytime coolings are comparably stronger than the same of the night over Arecibo.

The observed cooling in T_i trends seem to be related with the Debye radius, Debye number and Mean-Free-Path. At the altitude of F-region peak, there is a consistent correlation among those parameters with T_i Trends. Expansion of Debye radius is observed in the altitudes from 200-550 km. Above 550 km, shrinking is observed in Debye radius. This expansions are corresponding to the decreasing the number of particles in Debye sphere. It can be noted that number of particles in Debye sphere is decreasing over year irrespective of expansion or shrinking of Debye radius. But the Mean-Free-Path is

decreasing when there is shrinking or less expansion in Debye radius. At the altitude of large expansions of Debye radius trend, Mean-Free-Path is increasing over year. It is clear that long-term variations of T_i and other plasma parameters might have the influences by a common driver(s) but it needs further studies to understand processes that involved in expansion of Debye radius, decreasing number of particles in Debye sphere and changes in Mean-Free-Path by the cooling trends of T_i at least at the altitude where T_i is considerably equal/close to T_n (225-275 km). It is the altitude range where all the profiles of T_i trends from mid- and high-latitude have considerably similar cooling trends except the observations of Saint Santin.

At the altitude of 225-325 km, T_i is approximately equal to T_n . The estimated average T_i trend over Millstone Hill and Arecibo are -0.35 K/year and -1.775 K/year, respectively. At these altitudes, Strong cooling is exist over Arecibo than Millstone Hill even both do exist at mid-latitudes. Whereas, Arecibo has weak cooling trends than Millstone and other locations of mid- and high-latitude at the altitude range of 300-400 km; it is the altitude range where clear latitude dependency exist as cooling trends are as a function of latitudes. It can be mentioned that these altitudes appear abnormal at Arecibo as compared to altitudes above and below. For sake of discussion, latitudinal dependency is very clear among the Sondrestrom, Poker Flat, and Millstone if we remove the AO trends in the altitude range of 250-425 km. From high-mid latitude, the strength of cooling trends is decreasing. To bring this consistent behavior(it already exists among Sondrestrom, Poker Flat, and Millstone), the altitude range of ~ 350 -400 km is highlighted. Notably, there is also a structure around ~ 375 km in Poker Flat which is little similar to Arecibo's altitude structure in that altitude range with the maginude difference of ~ 2 K. Further studies are needed to understand these altitude structures in context to the dynamics and chemical composition if it exists with latitudinal dependency at those altitude ranges.

This latitudinal dependency may be starting to appear from 200 km as per the figure 10. From this altitude of 200 km to 400 km, the T_n trend was calculated to be 4-6 K/decade using neutral density trend (Akmaev, 2012). These values are 0.4-0.6 K/year which are lesser than Arecibo's T_i trends and comparable or greater than Millstone Hill's T_i trends of -0.35 K/year (Zhang & Holt, 2013). Even though the latitudinal dependency of T_i trends do exist in those altitude ranges but each location has its unique variabilities.

In the comparison of ISRs during daytime period, the observed T_i trends are having strong cooling (< -0.9 K/year) than the cooling from green house gases contributions by global simulation predictions (-0.2 K/year). In this case, additional drivers might be possible in cooling the upper atmosphere. It might be contributed by gravity wave (Oliver et al., 2013). Simulations show gravity waves can cool the upper atmosphere (Yigit & Medvede, 2009) and therefore it was speculated that the anticipated long-term gravity wave activity enhancement could lead to long-term cooling in the ionosphere (Oliver et al., 2013). Those gravity waves are speculated to be originated from ocean surfaces since there was a positive correlation between long-term trends of ion temperature and long-term relaxation in ENSO activity. It is shown in dashed pink line in the figure 11.

In figure 11, the time series of ion temperature (black-solid line) from 122-445 km and its residuals (green-plus-symbols) are shown. And the T_i trend line in green-solid line is shown for the altitude bin of 301-337 km where the daytime T_i trend almost matches with the same of Millstone Hill. ENSO MEI Index (pink-plus-symbols) and its trends (pink-dashed line-up to 2013 and pink-solid line-up to 2019) are shown in pink colors. Power dissipation index (PDI) of the hurricanes (red-dashed-dot line represents PDI and red-plus-symbols represents smoothed PDI) and its trend (red-solid line) over North Atlantic basin are shown in red colors. Notably, the magnitude of the negative trend of ion temperature is different from the magnitude of the negative trend of solar flux at 10.7 cm (blue color curve). In addition to the green house gases cooling, there may be also a possible contribution from gravity waves.

Based on ray tracing of the gravity waves over Arecibo, (Djuth et al., 2010) suggests that the source location possibly lies in the Atlantic ocean. This source would probably be linked with storm activities since there is an anti-correlation between the power dissipation index of hurricanes over the North Atlantic basin and the long-term trend of ion temperature. The increasing trend of power dissipation index of hurricanes indicates the increasing trend of hurricane activities so do storm activities. These increasing trends are also observed in sea-surface-temperatures and surface air temperatures (Wu & Wang, 2019). Responsible GWs are generated not alone by ocean since ENSO is a atmosphere-ocean coupling phenomenon (Huang et al., 2022). The power dissipation index (PDI) of hurricanes is increasing over time. PDI increase is negatively correlated with the T_i trends. Therefore, it could be possible that gravity waves might be generated by the systems associated with the interaction of the ocean and the atmosphere. These waves reach the upper atmosphere and might be contribute to the observed cooling ((Oliver et al., 2013)) by increasing the cooling trends of T_i green house gas cooling alone, explaining the discrepancy between the observed cooling and that predicted in the modeling studies.

Other ISR sites also have strong cooling trends but they are inland unlike Arecibo. It is not clear how the GWs associated with weather and ocean-atmosphere interaction influence the upper atmosphere of those regions. Further studies are needed to understand the latitudinal distribution of gravity wave flux and the contribution of gravity waves to the thermal structure of the upper atmosphere and to T_i trends. And also further studies are needed to investigate the source of the gravity waves and also whether those gravity waves are of lower atmospheric origin from weather phenomena and/or secondary waves from middle atmosphere.

Acknowledgments

Solar flux F10.7 and geomagnetic activity Ap index data are taken from https://lasp.colorado.edu/lisird/data/cls_radio_flux_f107/ and <http://wdc.kugi.kyoto-u.ac.jp/kp/index.html>, respectively. ISR data are taken from madrigal <http://openmadrigal.org> website. ENSO MEI index and Power Dissipation Index are taken from <https://psl.noaa.gov/enso/mei/> and www.epa.gov/climate-indicators, respectively. Authors gratefully thank the AO technical staff for their support in carrying out the ISR observations reported here and also thanking the people who does analysis and maintain madrigal database at AO. The AO is operated by the University of Central Florida under a cooperative agreement with the National Science Foundation, and in alliance with Ana G. Méndez-Universidad Metropolitana, and the Universities Space Research Association. Research at MIT Haystack Observation is supported in part by NSF Geospace Facility grant AGS-1952737 and NASA LWS program 80NSSC21K1315. The author would like to thank his colleagues Dr. Sravani Vaddi and Dr. Alison Smith for their help in manuscript reading and fruitful discussion.

References

- Akmaev, R. A. (2012). On estimation and attribution of long-term temperature trends in the thermosphere. *J. Geophys. Res.*, *117*, A09321.
- Akmaev, R. A., & Fomichev, V. I. (1998). Cooling of the mesosphere and lower thermosphere due to doubling of co2. *Ann. Geophys.*, *16*, 1501–1512.
- Bremer, J. (1992). Ionospheric trends in mid-latitudes as a possible indicator of the atmospheric greenhouse effect. *Journal of Atmospheric and Terrestrial Physics*, *54*, 1505–1511.
- Brum, C. G. M., Rodrigues, F. S., dos Santos, P. T., Matta, A. C., Aponte, N., Gonzalez, S. A., ... Robles, E. (2011). A modeling study of $f_o f_2$ and $h_m f_2$ parameters measured by the arecibo incoherent scatter radar and comparison with iri model predictions for solar cycles 21, 22, and 23. *J. Geophys. Res.*,

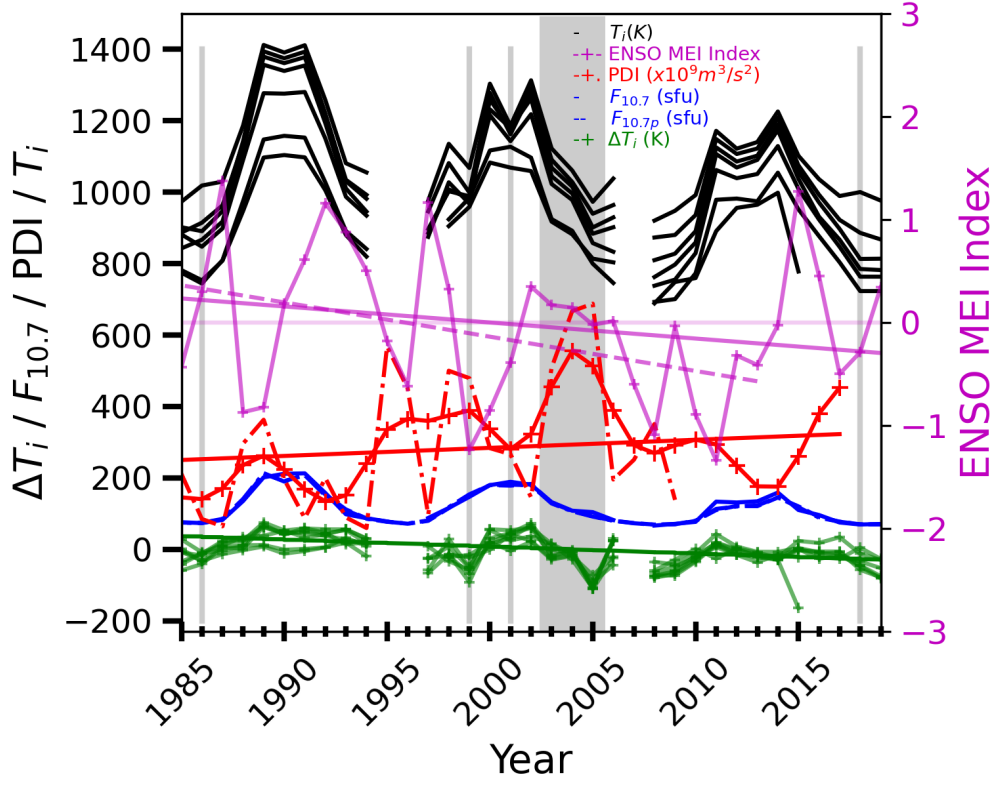


Figure 11. Time series of ion temperature (black-solid line) from 122-445 km and its residuals (green-plus-symbols). And the T_i trend line (green-solid line) of 301-337 km where the daytime T_i trend almost matches with the same of Millstone Hill. ENSO MEI Index (pink-plus-symbols) and its trends (pink-dashed line-upto 2013 and pink-solid line-upto 2019) along with power dissipation index (PDI) (red-dashed-dot line represents PDI and red-plus-symbols represents smoothed PDI) and its trend (red-solid line) over North Atlantic basin.

- 116, A03324.
- Brum, C. G. M., Tepley, C. A., Fentzke, J. T., Robles, E., dos Santos, P. T., & Gonzalez, S. A. (2012). Long-term changes in the thermospheric neutral winds over arecibo: Climatology based on over three decades of fabry-perot observations. *J. Geophys. Res.*, *117*, A00H14.
- Cai, Y., Yue, X., Wang, W., Zhang, S., Liu, L., Liu, H., & Wan, W. (2019). Long-term trend of topside ionospheric electron density derived from dmspdata during 1995–2017. *Journal of Geophysical Research: Space Physics*, *124*, 10708–10727.
- Cnossen, I. (2014). The importance of geomagnetic field changes versus rising CO_2 levels for long-term change in the upper atmosphere. *J. Space Weather Space Clim.*, *4*, A18.
- Cnossen, I., & Maute, A. (2020). Simulated trends in ionosphere-thermosphere climate due to predicted main magnetic field changes from 2015 to 2065. *J. Geophys. Res.: Space Physics*, *125*(3), e2773.
- Djuth, F. T., Zhang, L. D., Livneh, D. J., Seker, I., Smith, S. M., Sulzer, M. P., ... Walterscheid, R. L. (2010). Arecibo's thermospheric gravity waves and the case for an ocean source. *J. Geophys. Res.*, *115*, A08305.
- Donaldson, J. K., Wellman, T. J., & Oliver, W. L. (2010). Long-term change in thermospheric temperature above saint santin. *J. Geophys. Res.*, *115*, A11305.
- Emmert, J. T. (2015). Altitude and solar activity dependence of 1967–2005 thermospheric density trends derived from orbital drag. *J. Geophys. Res.: Space Physics*, *120*, 2940–2950.
- Emmert, J. T., Lean, J. L., & Picone, J. M. (2010). Record-low thermospheric density during the 2008 solar minimum. *Geophys. Res. Lett.*, *37*, L12102.
- Emmert, J. T., Picone, J. M., Lean, J. L., & Knowles, S. H. (2004). Global change in the thermosphere: Compelling evidence of a secular decrease in density. *J. Geophys. Res.*, *109*, A02301.
- Emmert, J. T., Picone, J. M., & Meier, R. R. (2008). Thermospheric global average density trends. *Geophys. Res. Lett.*, *35*, L05101.
- Goldston, R., & Rutherford, P. (1995). Introduction to plasma theory. *Bristol*, 13–16.
- Holt, J., & Zhang, S. (2008). Long-term temperature trends in the ionosphere above millstone hill. *Geophys. Res. Lett.*, *35*, L05813.
- Huang, Y., Yuan, N., Shi, M., Lu, Z., & Fu, Z. (2022). On the air-sea couplings over tropical pacific: An instantaneous coupling index using dynamical systems metrics. *Geophysical Research Letters*, *49*, e2021GL097049.
- Jacobi, C. (2014). Long-term trends and decadal variability of upper mesosphere/lower thermosphere gravity waves at midlatitudes. *Journal of Atmospheric and Solar-Terrestrial Physics*, *118*, 90–95.
- Keating, G. M., Tolson, R. H., & Bradford, M. S. (2000). Evidence of long term global decline in the earth's thermospheric densities apparently related to anthropogenic effects. *Geophys. Res. Lett.*, *27*, 1523–1526.
- Laštovička, J. (2021). Long-term trends in the upper atmosphere. *Chapter 17: Geophysical Monograph Series*.
- Laštovička, J., Akmaev, R. A., Beig, G., Bremer, J., & Emmert, J. T. (2006). Global change in the upper atmosphere. *Science*, *314*(5803), 1253–1254.
- Laštovička. (2015). Comment on “long-term trends in thermospheric neutral temperatures and density above millstone hill” by w. l. oliver et al.,. *J. Geophys. Res. Space Physics*, *120*, 2347–2349.
- Liu, H., Tao, C., Jin, H., & Abe, T. (2021). Geomagnetic activity effects on CO_2 -driven trend in the thermosphere and ionosphere: Ideal model experiments with gaia. *J. Geophys. Res.: Space Physics*, *126*, e2020JA028607.
- Livadiotis, G. (2019). Collision frequency and mean free path for plasmas described by kappa distributions. *AIP Advances*, *9*, 105307–105314.

- Mikhailov, A. V. (2006). Ionospheric long-term trends: can the geomagnetic control and the greenhouse hypotheses be reconciled?. *Ann. Geophys.*, *24*, 2533–2541.
- Ogawa, Y., Motoba, T., Buchert, S. C., Häggström, I., & Nozawa, S. (2014). Upper atmosphere cooling over the past 33 years. *Geophys. Res. Lett.*, *41*, 5629–5635.
- Oliver, W. L., Holt, J. M., Zhang, S.-R., & Goncharenko, L. P. (2014). Long-term trends in thermospheric neutral temperature and density above millstone hill. *J. Geophys. Res. Space Physics*, *119*, 7940–7946.
- Oliver, W. L., Holt, J. M., Zhang, S.-R., & Goncharenko, L. P. (2015). Reply to comment by jan lastovička on “long-term trends in thermospheric neutral temperature and density above millstone hill. *J. Geophys. Res. Space Physics*, *120*, 2350–2352.
- Oliver, W. L., Zhang, S.-R., & Goncharenko, L. P. (2013). Is thermospheric global cooling caused by gravity waves? *J. Geophys. Res. Space Physics*, *118*, 3898–3908.
- Qian, L., McInerney, J. M., Solomon, S. S., Liu, H., & Burns, A. G. (2021). Climate changes in the upper atmosphere: Contributions by the changing greenhouse gas concentrations and earth’s magnetic field from the 1960s to 2010s. *J. Geophys. Res.: Space Physics*, *126*, e2020JA029067.
- Rishbeth, H. (1990). A greenhouse effect in the ionosphere. *Planet. Space Sci.*, *38*, 945–948.
- Roble, R. G., & Dickinson, R. E. (1989). How will changes in carbon dioxide and methane modify the mean structure of the mesosphere and thermosphere? *Geophys. Res. Lett.*, *16*, 1441–1444.
- Santos, P. T., Brum, C. G. M., Tepley, C. A., Aponte, N., González, S. A., & Robles, E. (2011). Using incoherent scatter radar to investigate the neutral wind long-term trend over arecibo. *J. Geophys. Res.*, *116*, A00H13.
- Wu, R., & Wang, Y. (2019). Comparison of north atlantic oscillation-related changes in the north atlantic sea ice and associated surface quantities on different time scales. *J. Geophys. Res. Space Physics*, *40*, 2686–2701.
- Yiğit, E., & Medvede, A. S. (2009). Heating and cooling of the thermosphere by internal gravity waves. *Geophys. Res. Lett.*, *36*, L14807.
- Yue, X., Hu, L., Wei, Y., Wan, W., & Ning, B. (2018). Ionospheric trend over wuhan during 1947–2017: Comparison between simulation and observation. *Journal of Geophysical Research: Space Physics*, *123*(2), 1396–1409.
- Zhang, S.-R., & Holt, J. M. (2013). Long-term ionospheric cooling: Dependency on local time, season, solar activity, and geomagnetic activity. *J. Geophys. Res. Space Physics*, *118*, 3719–3730.
- Zhang, S.-R., Holt, J. M., Erickson, P. J., Goncharenko, L. P., Nicolls, M. J., McCready, M., & Kelly, J. (2016). Ionospheric ion temperature climate and upper atmospheric long-term cooling. *J. Geophys. Res. Space Physics*, *121*, 8951–8968.
- Zhang, S.-R., Holt, J. M., & Kurdzo, J. (2011). Millstone hill isr observations of upper atmospheric long-term changes: Height dependency. *J. Geophys. Res.*, *116*, A00H05.